SimBuild
2024

Eleventh National Conference of IBPSA-USA
Denver, Colorado
May 21 – 23, 2024

Local vs. Integrated Control Strategies for Heat Pump and PV Systems

Jeeye Mun[1], Seongkwon Cho[1], and Cheol-Soo Park[1]
[1]Seoul National University, Seoul, Republic of Korea

Abstract

This study presents a real-life implementation of online integrated control that simultaneously accounts for the dynamic relationships among an outdoor environment, a thermal zone, a heat pump (HP), and a photovoltaic (PV). The integrated control successfully finds the control variables of the HP (supply airflow rate, setpoint temperature) based on federated three Artificial Neural Network (ANN) models that predict the thermal zone's temperature, electricity produced by the PV, and energy consumption by the HP. Compared to the local control that determines control variables based on local information (room air temperature), the integrated approach could achieve an average 53.2% energy reduction.

Introduction

For a net-zero carbon society, it is crucial to focus on enhancing the net energy efficiency of an entire building. However, current building controllers in existing buildings generally treat each system as a local entity and perform control actions solely based on the local state information (Figure 1(a) Local control). This approach often leads to suboptimality as it overlooks the interplay between control actions and interconnected time-varying building systems such as stored heat in building structures and envelopes, cooling/heating of HVAC, and the energy generation system. For implementing the local control, Model Predictive Control (MPC) has been widely used in many studies (Zhao, & Magoules, 2012; Kumar, Aggarwal, & Sharma, 2013; Rastegarpour, Scattolini, & Ferrarini, 2021). The basic principle of MPC approach is to find optimal control variable(s) based on the outcome(s) predicted from the simulation model. The key aspects of MPC are developing an accurate simulation model and determining control variable(s) real-time that minimizes the objective function.

In contrast to the local control, an integrated controller considers the dynamic interactions among building systems and responds with an understanding of the time-varying states of the control target (Figure 1(b) Integrated control). It has been well-acknowledged that integrated control is superior compared to local control (Park & Augenbroe, 2013; Ahn et al. 2020). Ahn et al (2020) demonstrated a 21.6% reduction in cooling energy consumption using the integrated control for the variable refrigerant flow (VRF) system. However, the assessment of integrated control's performance has been limited to specific deterministic conditions.

Recognizing the inherent uncertainties that affect the thermal performance of building systems, it is imperative to consider the impact of these uncertainties on the energy-saving performance of building operation control (Macdonald 2001; de Wit 2002; Tian et al 2018). Several studies have proposed stochastic model MPC that optimizes control actions while accounting for uncertainties such as weather and occupancy (Mady et al. 2011; Ma, Matusko, and Borrelli 2015; Farina, Giulioni, & Scattolini 2016). Additionally, Li and Wang (2022) have compared the year-round performance of different MPC methods that optimized the utilization of PV power generation and battery storage systems under varying operating conditions.

This study presents a stochastic comparison of energy performance between the local and integrated control for a single thermal zone served by a HP and a PV panel. For this purpose, an experimental set-up was constructed as shown in Figure 2. Both the local and integrated approaches were implemented for seven days. In the local approach, control decisions rely on measured indoor room air temperature (Figure 3(a)), whereas the integrated approach finds control variables based on the dynamic relationships among the room, the PV, and the HP (Figure 3(b)).

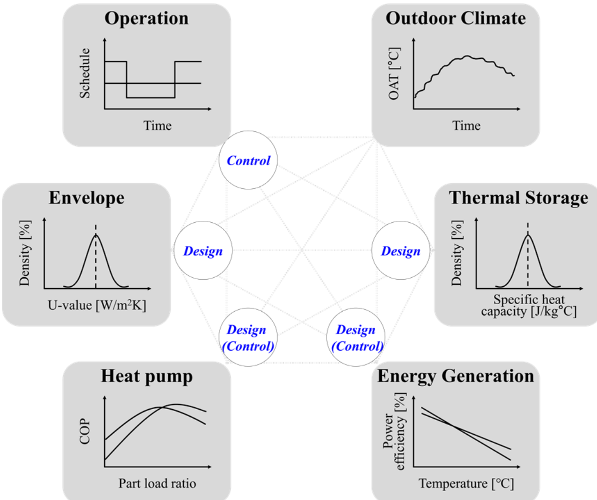

(a) As-is: Local

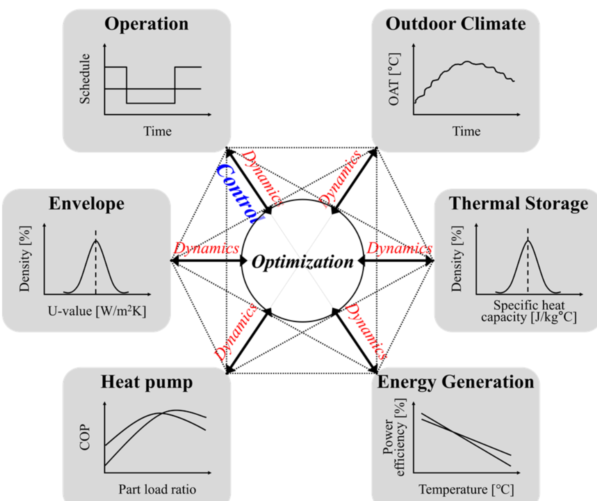

To-be: Integrated cooling control for interconnected building systems

Figure 1 Local vs. Integrated control

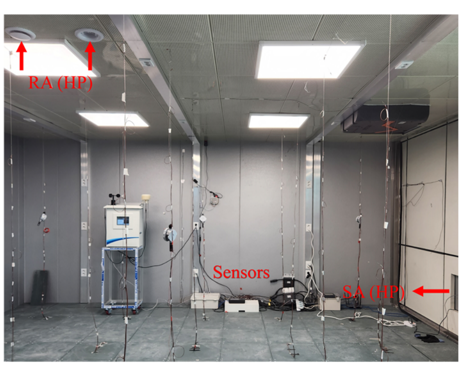

(a) Interior view

(b) Exterior view

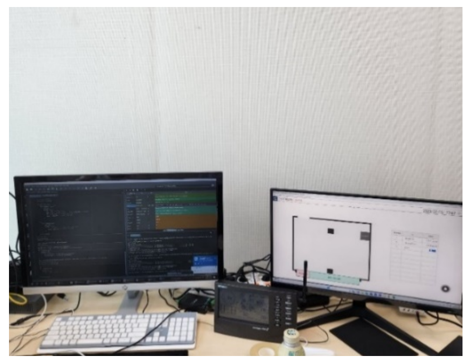

(c) Remote control

Figure 2 Target building

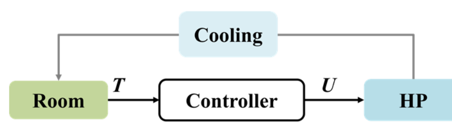

(a) Local control

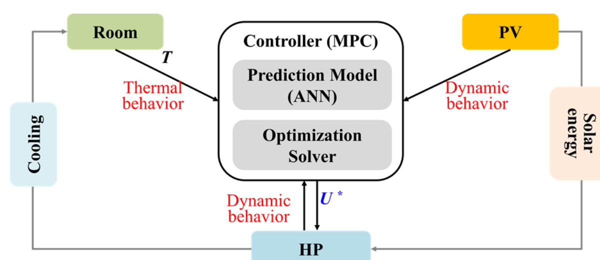

(b) Integrated control

Figure 3 Local vs. integrated controls for a thermal zone served by HP and PV

Experiment

The thermal zone is a 38.5m^2 room located on the third floor of an office building in Goyang, South Korea (Figure 2(a)). The zone borders the outdoor space on its east-southern side. The east-southern envelope consists of glazing, PV panels, an embedded HP, and precast concrete wall panels (Figure 2(b)). The HP system uses instantly generated solar energy from the PV system for cooling. To implement the real-time local and integrated controls, a remote control environment and network connection are established (Figure 2(c)).

Measured data are tabulated in Table 1: indoor air temperature (IAT), outdoor air temperature (OAT), solar radiation, PV surface temperature, electricity production by PV, HP operational data (return air temperature [RAT], supply air temperature [SAT], energy consumption), and control variables (HP supply airflow rate, HP setpoint temperature [SET]). The mean IAT (*T*) was computed based on measured air temperatures at five different spots in the room (Figure 4(a)). The PV incidence angle (*x3*) was calculated using the relevant physical formula (Reddy 2016). The mean PV panel surface temperature (*x4*) was derived from two data points measured at the top and bottom of the panel, respectively (Figure 4 (a), (b)). The maximum power consumption rate by the HP is 530W, while the peak electricity generation rate by the PV is approximately 500W.

In the cooling mode, the room's return air exchanges heat with the evaporator, and then the cooled air is supplied to the room (Figure 4(b)). In this study, the control variables are the supply airflow rate (*u1*) and the set-point temperature (*u2*). *u1* determines the supply air's volumetric rate, while *u2* controls the amount of heat exchange between the return air and the evaporator (Figure 4(b)). Please note that the HP's inverter is capable of modulating the compressor's speed based on the temperature difference between the return air and the set point (ΔT). The inverter operates at full power if ΔT is greater than 1°C. If ΔT is less than 1°C, the inverter adjusts the coil's heat absorption accordingly.

Table 1 List of collected data

	Variables	Unit	Index
State variables	Indoor air temperature (IAT) (average of *T-a*, *T-b*, *T-c*, *T-d*, and *T-e* (Figure 4(a))	°C	***T***
	Outdoor air temperature (OAT)	°C	*x1*
	Solar radiation	W/m^2	*x2*
	PV Incidence angle	degree	*x3*
	PV panel surface temperature (average of *x4-a* and *x4-b* Figure 4(a))	°C	*x4*
	Electricity production by PV	W	Q_{PV}
	HP On/Off	On/Off	*x5*
	Supply air temperature (SAT)	°C	*x6*
	Return air temperature (RAT)	°C	*x7*
	Electricity consumption by HP	W	Q_{HP}
Control variables	Supply airflow rate	Low / Medium / High	*u1*
	Set-point temperature (SET)	°C	*u2*

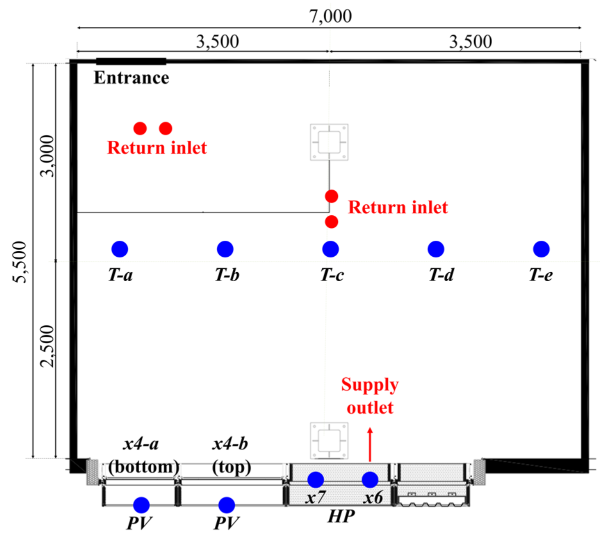

(a) Plan view of the thermal zone

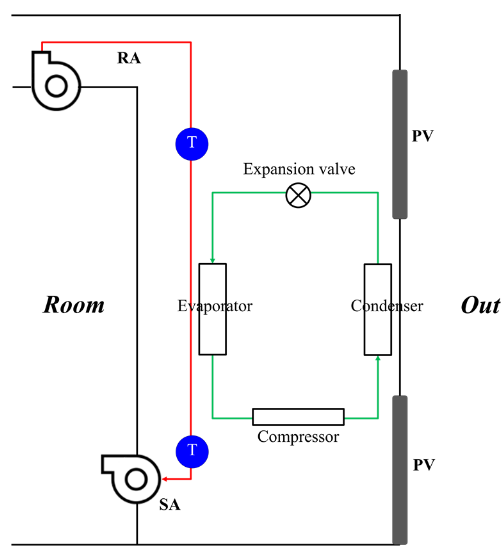

(b) Sectional view: HP and PV system

Figure 4 Schematic diagram of the experimental set-up

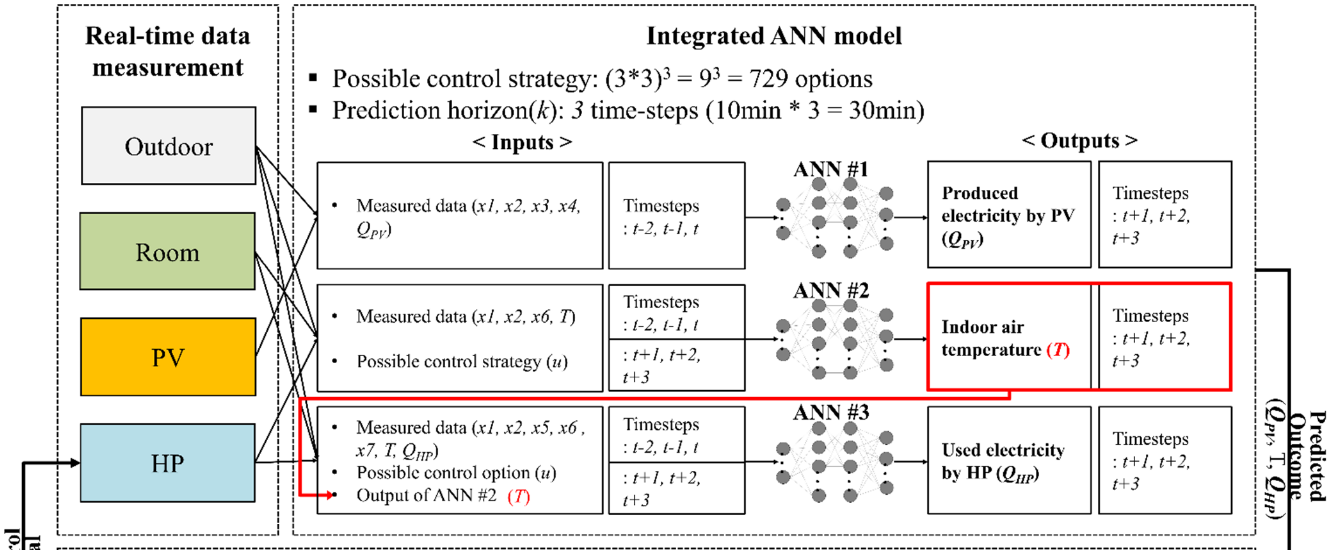

$$E_t = max(Q_{HP,t}(u_t) - Q_{PV,t}, 0)$$
$$U_{t+1} = \{u_{t+1}, u_{t+2}, \cdots, u_{t+k}\}$$
$$U^*_{t+1} = \underset{U_t}{argmin} \sum_{n=\{1,\cdots,k\}} E_{t+n} \quad s.t\ 23°C < \frac{1}{k} \sum_{n=\{1,\cdots,k\}} T_{t+n} < 25°C$$

u: control variables
T: indoor air temperature [°C]
Q_{HP} : used electricity by HP [W]
Q_{PV} : produced electricity by PV [W]
E: net electricity rate [W]
k: prediction horizon [timestep]

Figure 5 MPC for integrated control

Local Control vs. Integrated Control

The existing control, or the local control was implemented as shown in Table 2. The local control was based on the local information or the current IAT of the thermal zone (T). If T fell below 23°C, the heat pump was deactivated. Once T exceeded 25°C, the local control adjusted $u1$ to 'high' and $u2$ to 24°C. With T in the range of 23°C and 25°C, the local control maintained the previous time step's control variables. The sampling time was set to 10 min.

Table 2 Local control

T at *t*	***u1***	***u2***
T ≤ 23°C	HP Off	
23°C < ***T*** < 25°C	Same as *u1*, *u2* at *t-1*	
25°C ≤ ***T***	High	24°C

For implementing the integrated control, the authors employed MPC as shown in Figure 5. Firstly, three ANN models (ANN #1, #2, and #3, Figure 5) were developed to predict the electricity production by the PV, IAT, and the energy consumption by the HP, respectively. The sampling time and time horizon were set to 10 min and 30 min, respectively. The IAT predicted by ANN #2 is used as input for ANN #3 to predict the HP's cooling energy consumption. This strategy allows for the integration of information from ANN #2 into the functioning of ANN #3. For the development of the ANN models, the data collected between July 5 to 17 and 21 to 30, 2023 were used. The ANN models were validated by comparing the predicted values with the measured data in terms of mean absolute error (MAE) and coefficient of variation of the root mean absolute square error (CVRSME) (Table 3).

Table 3 Validation of the three ANN models during the test period (7/31)

	Time	ANN #1	ANN #2	ANN #3
		Q_{PV}	T	Q_{HP}
MAE	t+1	16.6 W	0.1 °C	14.0 W
	t+2	23.2 W	0.2 °C	22.3 W
	t+3	21.6 W	0.2 °C	26.7 W
CVRMSE	t+1	22.0 %	0.7 %	9.2 %
	t+2	26.7 %	1.0 %	8.3 %
	t+3	31.0 %	1.0 %	8.7 %

In Figure 5, the optimal control variables ($u1$, $u2$) in the integrated control were obtained using the exhaustive search method, while the local control follows the logic described in Table 2. Please note that a total of 9 control options are available at each time step, with 3 options for *u1* and another 3 options for *u2*. The options considered for the supply airflow rate (*u1*) were [low, medium, and high]. In response to the current return air temperature (*x7*), the options of the set-point temperature (*u2)* were adjusted every time-step as [*x7*-1, *x7,* and *x7*+1]. Consequently, for the three time steps of the prediction horizon, the search space becomes 729(=9^3). From the 729 predicted outcomes, the optimization solver could identify the control variables that minimize the net energy consumption while keeping the IAT within the target range of 23℃-25℃.

Results

The aforementioned local and integrated controls were experimented from September 1 to September 7, 2023. Each experiment consists of a series of 4-hour real-time implementations in an alternating order between morning and afternoon session. The results were categorized based on the operation time (AM/PM) and outdoor weather conditions into the six cases (Table 4).

Before attempting to compare the two controls, we compared the similarity of outdoor weather conditions under the local and integrated controls as shown in Figure 6. The differences in OAT [℃] (*x1*), solar radiation [W/m^2] (*x2*), and solar energy generated by PV [Wh] (Q_{HP}) were, on average, distributed around zero (Figure 6(a)-(c)).

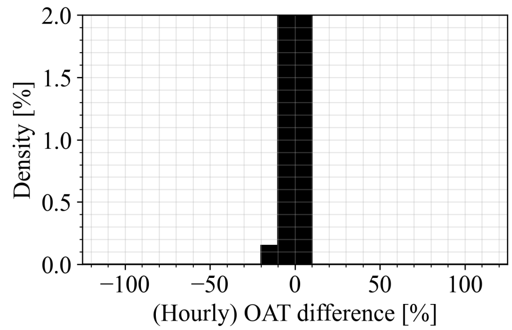

(a) Outdoor air temperature (OAT)

Table 4 Results of local and integrated controls

	Case 1		Case 2		Case 3		
	AM, sunny, mild temperature		**AM, rainy, mild temperature**		**AM, sunny, high temperature**		
Date	Sep 1	Sep 2	Sep 3	Sep 4	Sep 5	Sep 6	Sep 7
Control	Integrated	Local	Local	Integrated	Integrated	Local	Integrated
Average IAT[℃]	24.0	23.8	24.4	24.6	24.2	23.4	23.8
Average OAT [℃]	26.3	27.2	26.1	26.5	29.8	30.2	28.9
Average solar radiation [W/m^2]	578	526	257	285	434	516	578
Electricity consumption by HP [Wh]	1,259	1,294	556	666	1,412	2,081	1,600
Electricity production by PV [Wh]	1,295	1,148	313	407	963	1,189	1,335
Net energy consumption [Wh]	**378**	**571**	**410**	**357**	**541**	**892**	**491**
	Case 4		**Case 5**		**Case 6**		
	PM, sunny, mild temperature		**PM, rainy, mild temperature**		**PM, sunny, high temperature**		
Date	Sep 1	Sep 2	Sep 3	Sep 4	Sep 5	Sep 6	Sep 7
Control	Local	Integrated	Integrated	Local	Local	Integrated	Local
Average IAT [℃]	23.6	24.5	24.3	23.4	23.6	23.9	23.7
Average OAT [℃]	30.9	31.2	30.3	31.5	34.4	32.1	33.6
Average solar radiation [W/m^2]	593	546	234	307	600	278	610
Electricity consumption by HP [Wh]	1,649	691	927	1,923	2,158	1,460	1,438
Electricity production by PV [Wh]	229	259	220	263	242	182	199
Net energy consumption [Wh]	**1,440**	**447**	**740**	**1,663**	**1,916**	**1,300**	**1,270**

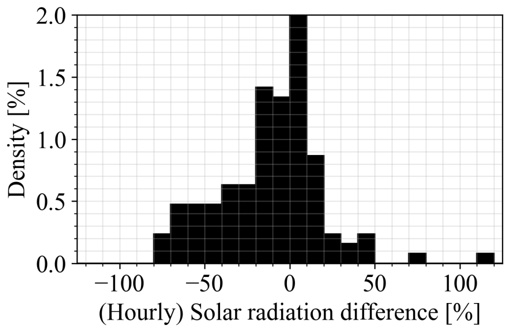

(b) Solar radiation

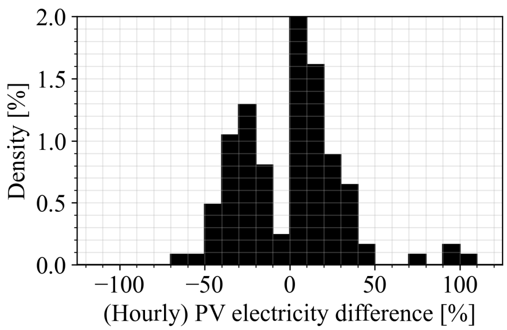

(c) Electricity production by PV

Figure 6 Hourly environmental conditions difference between local and integrated control (9/1-9/7)

Then, the performance difference, $\triangle P$ between the local and integrated control was assessed as shown in Equation (1).

$$\triangle P = \left(\frac{E_{t,local} - E_{t,integrated}}{E_{t,local}}\right) \quad (1)$$

$E_{t,integrated}$: net energy consumption of the integrated control

$E_{t,local}$: net energy consumption of the local control

Figure 7(a) and (b) illustrates the stochastic variation in the hourly energy consumption over a week (September 1-7, 2023) under the two control methods. Under the local control, the hourly net electricity consumption shows the highest density in 160-180Wh (Figure 7(a)). In contrast, the net electricity consumption under the integrated control revealed a highest density in the range of 20-40Wh (Figure 7(b)). Figure 7(c) shows the distribution of $\triangle P$ between the local and integrated control. The variation of $\triangle P$ was quantified using the median and the interquartile range (IQR), because IQR, representing the difference between the first quantile and the third quantile of a dataset, provides information about the spread of the central 50% of the data and is robust to outliers. The variation of $\triangle P$ demonstrates an average of 53.23% and an IQR of 36.7% (Figure 7). Throughout most of the experimental periods, it was observed that the net energy consumption of the integrated control was far less than that of the local control (Table 4, Figure 7). In addition, please note that the degree of superiority of the integrated control is strongly stochastic, influenced by the outdoor weather conditions.

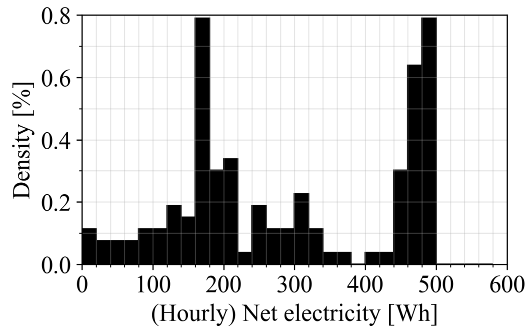

(a) Net energy consumption under local control

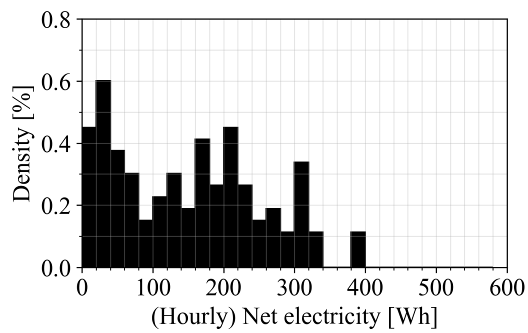

(b) Net energy consumption under integrated control

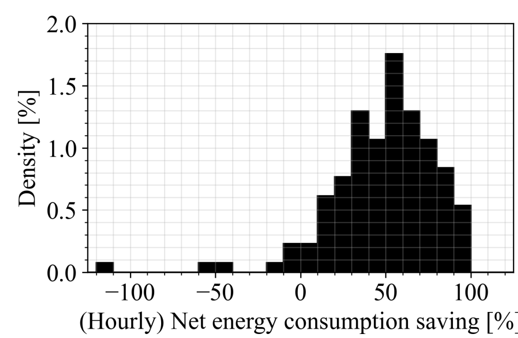

(c) Performance difference between local and integrated control

Figure 7 Stochastic variation of local and integrated control (Sep 1- Sep 7, 2023)

For the illustration purpose, Figure 8 presents the time-series data of Case 3 (Table 4) for integrated (Sep 5) and local (Sep 6) control operations from 8:00 to 12:00. It showcases OAT, IAT, RAT, SET, electricity consumption by the HP, and electricity production by the PV. Both the local and integrated control effectively maintained the IAT within the desired range (Figure 8 (a), (c)). During the integrated control operation, the electricity consumption by the HP continuously fluctuated according to the optimized control variables (Figure 8(d)). The integrated control significantly reduced cooling energy consumption (local: 2,081Wh, integrated: 1,412Wh), and accordingly, 4-hour net energy consumption is as follows: (local: 892Wh, integrated: 541Wh) (Table 4: Case 3). Figure 8 (e) illustrates a comparison of the net energy consumption between the local and integrated control. The potential energy savings of the integrated control can be attributed to the following aspects:

- The local control had to supply cooling continuously even when the IAT was within the desired range because it was not capable of describing the dynamic behavior of IAT. In other words, because the local control does not know the dynamic relationship between the provided cold and IAT at a future timestep, it had to follow the pre-determined control logic as shown in Table 2. In contrast, the integrated control effectively maintained the IAT within the desired range by predicting the thermal dynamics of the HP system and the indoor room. (Figure 8 (c)).
- The integrated control effectively minimized net energy consumption by leveraging three ANN models that are capable of predicting future room air, PV electricity production, and HP electricity consumption, respectively. In other words, the integrated control can find a way to make the best use of the PV electricity to assist with cooling the air within the room, via the heat pump (Figure 8 (d)).

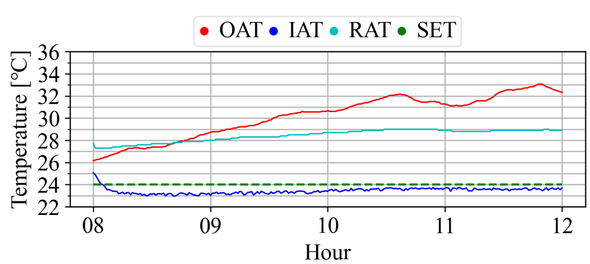

(a) OAT, IAT, RAT and SET under local control (Sep 6)

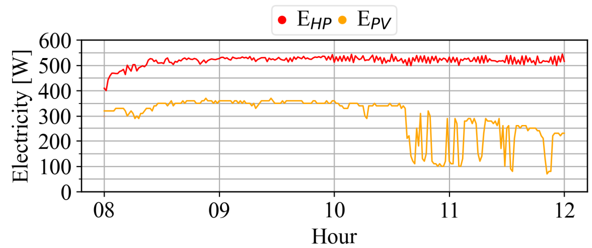

(b) Q_{HP} and Q_{PV} under local control (Sep 6)

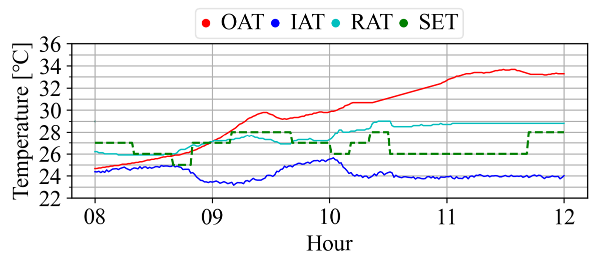

(c) OAT, IAT, RAT and SET under integrated control (Sep 5)

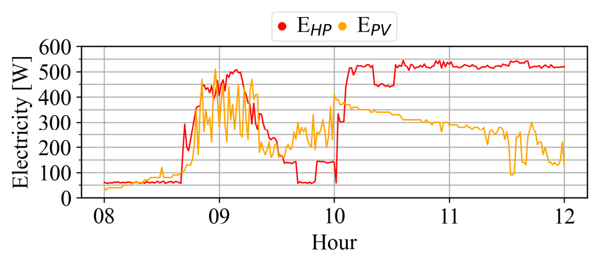

(d) Q_{HP} and Q_{PV} under integrated control (Sep 5)

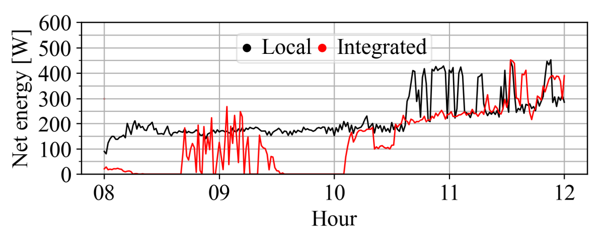

(e) Net energy consumption of two controls

Figure 8 Comparison between local and integrated control (Case 3)

Conclusion

Many existing studies have primarily focused on a local control problem, relying exclusively on local state information such as IAT. In contrast, this study explored the potential of an integrated control that incorporates the dynamics of the thermal zone (room), the outdoor environment, the heat pump (HP), and photovoltaic (PV) systems.

Using a simple ANN-based MPC, the study successfully implemented the real-time integrated cooling control for the given thermal zone. The in-situ experiment was conducted over a week in a real-life building and the results demonstrated a substantial superiority of the integrated control over the local control. The integrated control yielded a reduction in net energy consumption, averaging 53.23% with an interquartile range (IQR) of 36.7% compared to the local control.

This outcome can be attributed to three key factors of the integrated control: 1) a capability to predict room air change in a next time horizon, 2) a capability to predict PV energy generation during the future time horizon, and 3) comprehension of the HP's energy use, e.g. part-load, COP, and (4) understanding of the interwoven three different dynamics between the thermal zone, the PV and the HP. The study emphasizes the importance of adopting an integrated approach for a variety of building energy systems in daily practice.

Acknowledgment

This work was supported by Korea Institute of Energy Technology Evaluation and Planning (KETEP) grant funded by the Korea government (MOTIE) (20202020800030, Development of Smart Hybrid Envelope Systems for Zero Energy Buildings through Holistic Performance Test and Evaluation Methods and Fields Verifications).

References

Ahn, K., Kim, K. J., Song, K., & Park, C. S. (2020). Local vs. integrated control of a variable refrigerant flow system using artificial neural networks. Science and Technology for the Built Environment, 26(8), 1117-1131.

Ahn, K. U., Park, C. S., Kim, K. J., Kim, D. W., & Chae, C. U. (2022). Hybrid model using Bayesian neural network for variable refrigerant flow system. Journal of Building Performance Simulation, 15(1), 1-20.

De Wit, S., & Augenbroe, G. (2002). Analysis of uncertainty in building design evaluations and its implications. Energy and buildings, 34(9), 951-958.

Drgoňa, J., Arroyo, J., Figueroa, I. C., Blum, D., Arendt, K., Kim, D., Olle, E. P., Oravec, J., Wetter, M., Vrabie, D. L., & Helsen, L. (2020). All you need to know about model predictive control for buildings. Annual Reviews in Control, 50, 190-232.

Farina, M., Giulioni, L., & Scattolini, R. (2016). Stochastic linear model predictive control with chance constraints–a review. Journal of Process Control, 44, 53-67.

Hensen, J. (2003). Paper Preparation Guide and Submission Instruction for Building Simulation 2003 Conference. Eindhoven, The Netherlands.

Kim, Y. M., Ahn, K. U., & Park, C. S. (2016). Issues of application of machine learning models for virtual and real-life buildings. Sustainability, 8(6), 543.

Kim, Y. S., & Park, C. S. (2023). Real-time predictive control of HVAC systems for factory building using lightweight data-driven model. Journal of Building Performance Simulation, 1-19.

Kumar, R., Aggarwal, R. K., & Sharma, J. D. (2013). Energy analysis of a building using artificial neural network: A review. Energy and Buildings, 65, 352-358.

Li, H., & Wang, S. (2022). Comparative assessment of alternative MPC strategies using real meteorological data and their enhancement for optimal utilization of flexibility-resources in buildings. Energy, 244, 122693.

Ma, Y., Matuško, J., & Borrelli, F. (2014). Stochastic model predictive control for building HVAC systems: Complexity and conservatism. IEEE Transactions on Control Systems Technology, 23(1), 101-116.

Macdonald, I., & Strachan, P. (2001). Practical application of uncertainty analysis. Energy and Buildings, 33(3), 219-227.

Mady, A. E. D., Provan, G., Ryan, C., & Brown, K. (2011, August). Stochastic model predictive controller for the integration of building use and temperature regulation. In Proceedings of the AAAI conference on artificial intelligence (Vol. 25, No. 1, pp. 1371-1376).

Mitchell, J. W., & Beckman, W. A. (1995). Instructions for IBPSA Manuscripts. SEL, University of Wisconsin, Madison USA.

Moghaddas-Zadeh, N., Farzaneh-Gord, M., Ebrahimi-Moghadam, A., & Bahnfleth, W. P. (2023). ANN-based procedure to obtain the optimal design and operation of the compression chiller network–Energy, economic and environmental analysis. Journal of Building Engineering, 72, 106711

Park, C. S., & Augenbroe, G. (2013). Local vs. integrated control strategies for double-skin systems. Automation in construction, 30, 50-56.

Ra, S. J., Kim, J. H., & Park, C. S. (2023). Real-time model predictive cooling control for an HVAC system in a factory building. Energy and Buildings, 285, 112860.

Rastegarpour, S., Scattolini, R., & Ferrarini, L. (2021). Performance improvement of an air-to-water heat pump through linear time-varying MPC with adaptive COP predictor. Journal of Process Control, 99, 69-78.

Reddy, T., Kreider, J. F., Curtiss, P. S., & Rabl, A. (2016). Heating and cooling of buildings: principles and practice of energy efficient design. CRC press.

Tian, W., Heo, Y., De Wilde, P., Li, Z., Yan, D., Park, C. S., Feng, X., & Augenbroe, G. (2018). A review of uncertainty analysis in building energy assessment. Renewable and Sustainable Energy Reviews, 93, 285-301.

Zhao, D., Zhong, M., Zhang, X., & Su, X. (2016). Energy consumption predicting model of VRV (Variable refrigerant volume) system in office buildings based on data mining. Energy, 102, 660-668.

Zhao, H. X., & Magoulès, F. (2012). A review on the prediction of building energy consumption. Renewable and Sustainable Energy Reviews, 16(6), 3586-3592.